Controlled electroplating for high-aspect-ratio zone-plate fabrication

A. Holmberg,[a] M. Lindblom, and H. M. Hertz
*Biomedical and X-Ray Physics, Department of Applied Physics, Royal Institute of Technology/Albanova,
SE-10691 Stockholm, Sweden*

The authors report a method for monitoring, control, and end-point detection of electroplating in nanostructures. The method is demonstrated on nickel plating into polymer molds, which is an important process in the fabrication of soft x-ray zone-plate diffractive optics. The lack of reproducibility presently limits the achievable nickel aspect ratio and, thus, reduces the zone-plate diffraction efficiency. The reported method provides reproducible plating via real-time control of the plating rate. It combines *in situ* light transmission measurements with current measurements to determine the thickness of the growing layer. The accuracy of the thickness prediction was better than $\pm4\%$ (1σ) for $100-300$ nm nickel layers. Furthermore, a slight change in the light transmission signal indicates when a gratinglike zone-plate structure is slightly overplated and the plating should be stopped. This end-point detection provides the optimal filling of high-aspect-ratio molds for improved diffraction efficiency. © *2006 American Vacuum Society.* [DOI: 10.1116/1.2362761]

I. INTRODUCTION

Zone plates and other diffractive optical elements are becoming increasingly important for x-ray imaging, focusing, and spectroscopy.[1] A high aspect ratio is necessary to obtain high diffraction efficiency for these repetitive and narrow-linewidth structures. A critical step in the fabrication process is the deposition of the x-ray-optic material, which today mainly is performed by electroplating in a mold. In the present article we introduce *in situ* light transmission measurement methods, which allows the accurate control of the electroplated thickness leading to the reproducible fabrication of high-aspect-ratio structures.

Zone plates are diffractive optical elements with multiple diffraction-order foci.[2] They consist of several hundreds of alternating transparent and opaque or phase-shifting circular zones, with radially decreasing zone widths. In soft x-ray microscopy based on zone plates, the spatial resolution is directly proportional to the outer zone width. Typical data for present high-resolution soft x-ray zone plates are 50 μm diameter, 500 zones, and an outer zone width of $20-50$ nm. The diffraction efficiency of the zone plate depends on both the material and the thickness of material.[3] In the soft x-ray regime nickel is well suited since the phase/absorption ratio is high, allowing the fabrication of phase zone plates with high diffraction efficiency. The optimum zone height varies with wavelength but, in general, the theoretical first-order diffraction efficiency scales with nickel height, resulting in, e.g., a diffraction efficiency of 23.5% for 250 nm high nickel zones at a wavelength of $\lambda=2.4$ nm. A high diffraction efficiency directly corresponds to shorter exposure times and lower dose in x-ray microscopy. The desire for both resolution and high diffraction efficiency explains the need for the high-aspect-ratio processing of repetitive and narrow-linewidth structures. In addition, even higher aspect ratios are valuable, both for improved diffraction efficiency for hard x-ray diffractive optical elements[4] and for increased higher-order diffraction efficiencies in the soft x-ray regime.[5]

These special demands on the zone plates are the driving force for the development of suitable nanofabrication processes. The patterning is typically performed by electron-beam lithography followed by different plasma etch steps to provide a mold. The mold is then filled with the desired zone-plate material by electroplating, after which the mold is removed. Electroplating is chosen for its possibility to form higher aspect ratios than, e.g., lift-off based evaporation deposition methods. Several groups have improved different aspects of the processes for zone-plate fabrication. For example, commercial electron-beam lithography systems have been modified for high-placement-accuracy electron-beam lithography.[6] Cryogenically cooled inductively coupled plasma etching has been used to improve the anisotropicity of the plating mold.[7] The mechanical stability of the mold material has been improved by x-ray cross linking of the polymers.[8] In terms of resolution, 15 nm outer zone width zone plates have been fabricated.[9] For zone plates, for which equal emphasis has been on resolution and efficiency, 20 nm outer zone width combined with 170 nm zone height and a measured diffraction efficiency of 9.2% at $\lambda=2.4$ nm has been reported.[10]

The electroplating process step presently limits the achievable aspect ratio. The mold structures (the zones) may collapse due to capillary forces when submerged into the plating bath. Thus, it is important to limit the aspect ratio of the mold so that it can withstand the electroplating process step better. In order to optimize the diffraction efficiency it is then clearly desirable to fill the mold as completely as possible. In the present article we describe two measurement methods that allows a complete fill of the mold via *in situ* measurements of plating thickness during the plating process. These methods give increased control of the electroplating process and result in reproducible fabrication of high-aspect-ratio zone plates.

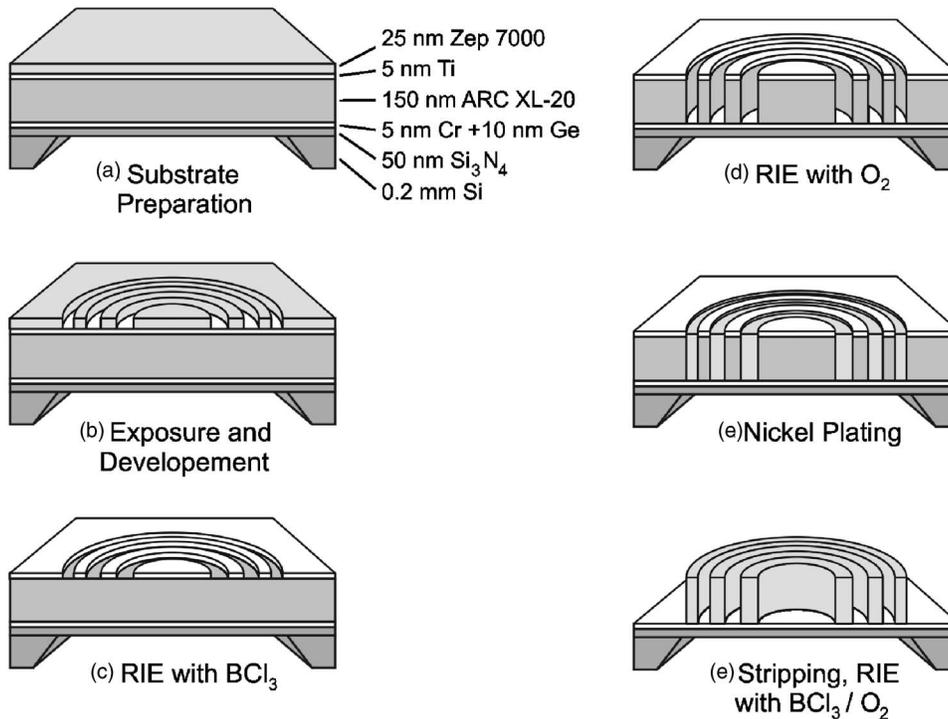[a]Electronic mail: anders.holmberg@biox.kth.se

FIG. 1. Process steps for fabrication of high-aspect-ratio zone plates.

II. FABRICATION

The zone plates are electroplated in a mold fabricated with electron-beam lithography and reactive ion etching (RIE) from a trilayer resist system.[11] The process steps are shown in Fig. 1. A plating base and the trilevel resist system are prepared on a 50 nm x-ray-transparent Si_3N_4 membrane supported by a silicon frame. This is done with standard vapor deposition and spin coating techniques. After exposure and development, BCl_3 and O_2 RIE process steps completes the plating mold. The sample is then electroplated and finally the mold is removed with another set of BCl_3 and O_2 RIE steps. Further details, including process parameters and conditions, are found in Ref. 11.

The key issue for the electroplating is to obtain the right thickness. An overfilling of the plating mold makes it impossible to remove the mold afterwards and results in a useless zone plate. On the other hand, to achieve the highest possible diffraction efficiency, it is important to fill the mold entirely. Before the introduction of the control methods described in the present article the electroplating rate could fluctuate up to $\pm20\%$ between different samples. Thereby the plated thickness varied with the same percentage.

According to basic electroplating theory,[12] the deposited mass m is proportional to the current via Faraday's law,

$$m = \eta(A_{wt}It)/nF, \tag{1}$$

where A_{wt} is the atomic weight, I is the current, t is the time, n is the number of electrons involved in the ion transfer, F is Faradays constant, and η is the current efficiency, i.e., the fraction of the total charge input that is used for deposition of metal. Thus, in principle, the deposited mass is known if the current and time is measured. However, the deposition rate (m/t) can vary greatly with position, and therefore the plated thickness at a local position is not accurately known. For plating-through-mask structures this has been discussed in, e.g., Ref. 13. In addition, the area of the structures are often not well known. Normally several zone plates are exposed in a dose test on the same SiN membrane, giving different line-to-space ratios, and this influences the total plating area. Especially for narrow-linewidth structures, where the fabrication process is used at its limits, the result of a dose test means overexposed in combination with underexposed structures. Because of the high-aspect-ratio mold it is also difficult to analyze whether a structure on the sample is etched all the way through the mold layer into the plating base, which further increases the uncertainty in the plating area. Another example is the electroplating of large condenser zone plates fabricated with a stitched writefields method.[14] In this case the pattern is severely distorted due to electron-beam-focus variation within individual writefields. This also results in difficulty in estimating the plating area.

The experimental arrangement and the *in situ* control methods discussed in Secs. III–V were introduced to alleviate these problems so that reproducible and accurate plating can be obtained for structures with unknown area. The control techniques relies on the combination of current control and visible light transmission measurements through the Si_3N_4 membranes during the electroplating.

III. ELECTROPLATING ARRANGEMENT

The electroplating is performed with a sulfamate-type nickel solution, where the plating process is driven by an applied current between an anode and the cathode (the sample). For the light transmission measurements the plating
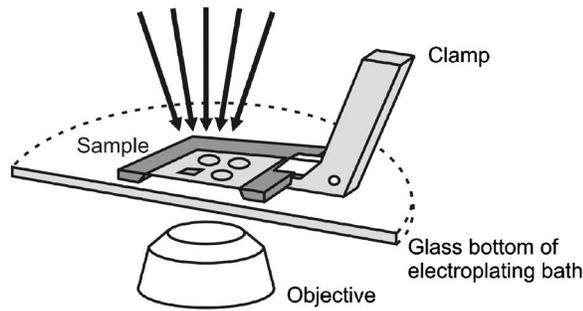
FIG. 2. Experimental arrangement for the optical transmission measurements during the electroplating process.

FIG. 4. Light transmission as a function of time during electroplating.

bath is mounted onto an inverted microscope (Nikon TS100), as shown in Fig. 2. The bath has an integrated glass window in the bottom allowing the observation of the sample from below. The top of the bath is open, giving access for the condenser illumination.

For image collection, a black-and-white, digital video camera is used (Sony XCD-X710). It is operated at 50 frames/s with 512×384 8 bit pixels. Figure 3 shows an image from an on-going plating. In the present arrangement the mechanical drift requires that the transmission data are acquired from a structure with dimensions of a few tens of micrometers. Since the zone plate itself does not contain any structures large enough for reliable transmission data the rectangular structure to the left in Fig. 3 is added. It contains a grating with 50 nm lines and spaces and a $50 \times 50 \ \mu m^2$ square. The light intensity data is collected from the central part of the square. The resolution in the image is presently limited to about 1 μm. The current through the sample is measured with a high-resolution picoammeter (Keithley 6485). A software application written in LABVIEW is used for video monitoring, data collection, and the *in situ* analysis. Transmission-signal data can be taken from an arbitrary area within a video frame. The data acquisition rate for the current and the transmission data are typically 1 Hz.
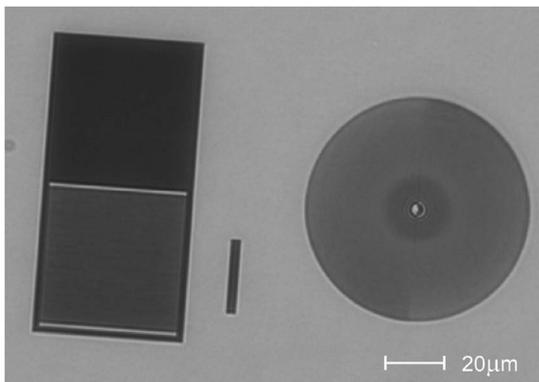
IV. *IN SITU* THICKNESS CONTROL

FIG. 3. Transmission light-microscope image recorded during plating of structures on a Si_3N_4 membrane. To the right, a 75 μm diameter, 50 nm outermost zone plate. To the left, a test pattern containing a 100 nm period grating (upper) and a large square (lower).

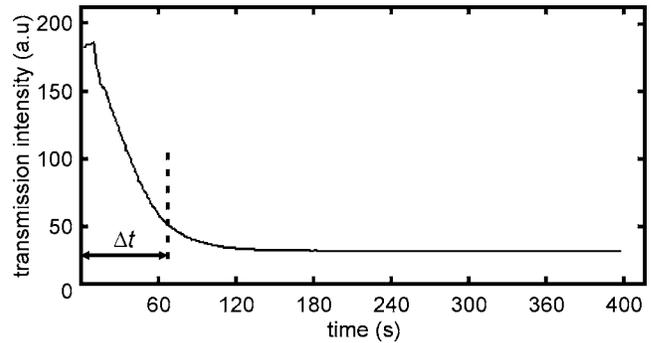The transmission of light through the growing nickel layer and the Si_3N_4 membrane with its plating base can be described with multilayer theory including multiple reflections and absorption. Following the standard matrix model approach this is a straightforward calculation.[15] However, the growing nickel structures will initially alter the background condition due to the shading of incoming light and reflections at the back side of the structures. Due to strong absorption in the metal layers, the interference effects from the multilayer reflections are small and the background change dominates. An example of a measured transmission curve is shown in Fig. 4. After a certain time Δt the background is approximately constant. The magnitude of the background change varies with the structure layout on the membrane and experiments show that the change is negligible after the first tens of plated nanometers. For the thickness control we therefore exclude the first tens of nanometers. After this initial state the multilayer effect is no longer measurable and the light intensity transmitted through the nickel layer has therefore been modeled by an exponential decay with respect to nickel thickness.

The entities that are measured during plating are the current through the sample $i(t)$ and the transmitted light intensity through the nickel layer $T(t)$. According to our model the transmitted intensity can be related to the thickness of the nickel through an exponential function,

$$T(d(t)) = A + Be^{-\alpha_d d(t)}, \quad (2)$$

where A is the background level, B is the incoming light intensity, and α_d is a material-specific attenuation coefficient, which is experimentally calibrated. The dependence on time, t, has been written out to emphasize that it is the time and not the thickness $d(t)$ that is measured. To be able to relate the thickness to the measured current, it is assumed that the plating area of the sample, the current distribution, the density, and the current efficiency are constant in time. With these assumptions the plated thickness at one point of the sample will be proportional to the total charge transferred to the sample, according to Eq. (1) and the thickness can be expressed as a function of the time-dependent current as

$$d(t) = k \int_{t_0}^{t} i(t')dt', \tag{3}$$

where k is an unknown constant and t_0 is the start time. Inserting this expression in Eq. (2) results in

$$T(t) = A + Be^{-\alpha_d k \int_{t_0 + \Delta t}^{t} i(t')dt'}. \tag{4}$$

The transmission $T(t)$ and the current $i(t)$ are constantly measured and A, B, and k can be determined by a nonlinear fit. When k is known the thickness at any given time can be calculated using Eq. (3). The delay Δt indicates the time after which the nickel has reached the thickness required for the data to be used in the nonlinear fit. This time is determined iteratively, beginning with an initial estimate based on the expected plating rate and our experience of a suitable minimum thickness for the nonlinear fit. When the plating has proceeded for longer than the estimated time and the rate calculation has begun, Δt is continuously adjusted based on the calculated plating rate. Note that in Eq. (3) Δt does not appear in the integration boundary. Here the total charge transferred to the sample from the start of the plating is used for calculating the thickness. The initial data is only left out in the determination of the proportionality constant k.

The transmission-current method has been evaluated on a large set of glass samples. The plated nickel thicknesses were measured with a line scan profilometer (Tencor P15). These measurements are more accurate on glass than on Si_3N_4 membranes, since no error is introduced due to membrane deformation caused by stress in the film. The samples had 5 nm Cr and 10 nm Ge and a sufficiently thick mold layer for the nominal plating thickness. Circular areas with diameters between 180 and 210 μm for the plating where prepared in the mold by RIE through a metal mask. The variation in diameters gives an area variation that is comparable with that on real zone-plate samples. The plating rate was approximately 25–35 nm/min. To avoid multilayer effects and changing background intensity, data was used only from when the nickel layers were thicker than 35 nm. Figure 5 shows profilometer-measured thicknesses as a function of the predicted thickness by the transmission-current method. The overall accuracy of the predicted thickness is $\pm 4\%$ (1σ) with respect to all plated samples. The nominal thicknesses ranged from about 100 to 300 nm, which corresponds to the interval of interest for our fabrication.

V. END-POINT DETECTION

The thickness control method demonstrated in Sec. IV gives good knowledge of the plating rate in large structures, such as the square shown in Fig. 3, and can be used as feedback signal to adjust plating rate or to decide when to terminate the plating. However, due to nonuniform current distribution resulting from the geometry and aspect-ratio variation of the structures, the nickel height may be lower in the narrow-linewidth zones than in the larger structure. An end-point detection method was therefore introduced, which gives an accurate detection of when the mold for the critical structure, i.e., the zone-plate optics, is filled.
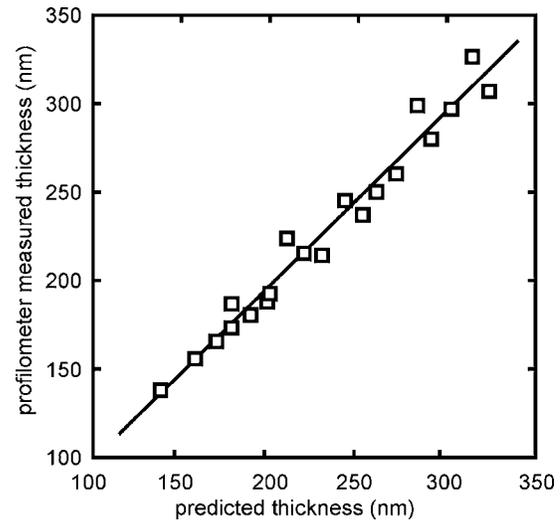

FIG. 5. Correlation between the thickness predicted by the *in situ* transmission-current based method and profilometer measurements.

The end-point method utilizes the slight change in light transmission that occurs when the plated metal starts to grow over the gratinglike plating mold. When the metal fills the mold, it grows anisotropically upwards, limited by the mold walls. At some point the metal reaches the mold edge and starts to grow isotropically over the mold. Figure 6 shows an example of a measured transmission curve and a schematic that illustrates the different phases (A–D) during the plating. At A the nickel thickness is below the opaque thickness and the signal decays exponentially. At B the thickness is so large that the Ni is nearly opaque and the signal starts a linear decay. We assume that this linear decay is due to polarization effects, but it has not been further investigated. At C the mold is filled and the signal drops as the metal starts to grow isotropically over the mold. The transmission-signal sam-
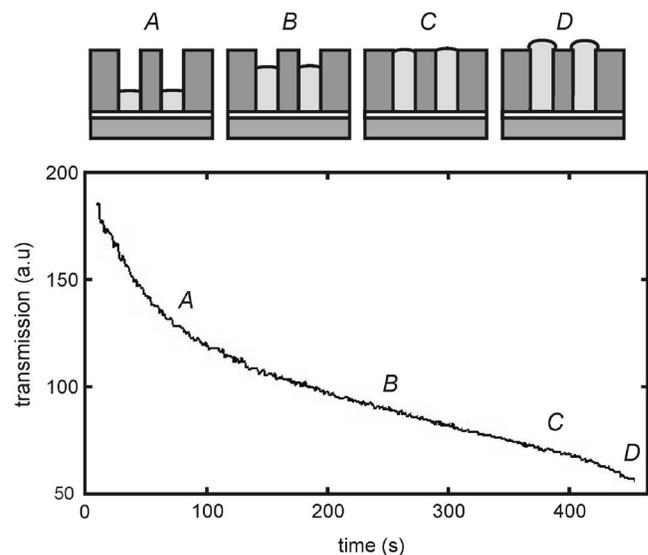

FIG. 6. Experimental recording of the transmission signal through a grating. The different fill ratios are shown schematically on top. Note the drop in intensity at D, which is used for end-point detection.
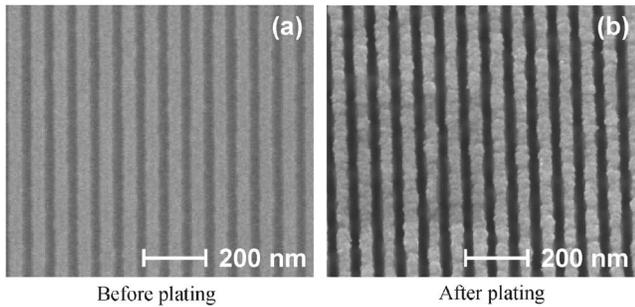
FIG. 7. Scanning electron microscope images of a grating before and after plating with end-point detection. (a) shows 50 nm bright mold lines and 50 nm dark spaces before plating. (b) shows the slightly overplated mold where the nickel is bright and the mold dark.

pling interval was 1 s and each sample is taken as an average over 30×30 pixels^2, which corresponds to an area of 10×10 μm^2 on the grating.

So far we have not developed an analytical model that describes the light attenuation through a gratinglike structure during plating. We expect that the variation in line-to-space ratio of the structures makes such a model difficult to rely on. For the end-point detection, however, inspection of the transmission curve (see Fig. 6) is sufficient to identify and terminate the plating at the final dip of the curve. Alternatively, a software routine that triggers on the dip can be used.

Figure 7 shows scanning electron microscope images of the grating measured in Fig. 6 before and after plating. The nominal line and space widths of the grating is 50 nm, and the mold height is 160 nm. In the plated mold [Fig. 7(b)] one can observe how individual grains start to grow over the mold edge. This slight overplate has not been observed to have any negative effect on the final removal of the mask with the BCl$_3$ and O$_2$ etch.

VI. CONCLUSIONS

Two methods to control electroplating for the fabrication of zone plates have been demonstrated. First, we have shown that the plated thickness on samples with unknown area can be controlled by correlating the visible light transmission signal with the total current passing the sample during plating. Second, an end-point detection method for the accurate filling of a gratinglike mold was demonstrated. The method utilizes the slight change in light transmission that occurs when the plated metal starts to grow isotropically over the plating mold.

Our methods for improved electroplating control demonstrate the possibility to reproducibly fill high-aspect-ratio molds. For many applications this is sufficient. In addition, the accurate filling that is obtained with the end-point detection method suggests the possibility to stack zone plates on top of each other without the need of mechanical polishing between each processed layer. Stacked zone plates have been proposed as a means to obtain the very high aspect ratios necessary for volume zone plates,[16] which operate with high efficiency at higher diffraction orders. Such zone plates would improve resolution and decrease exposure time in x-ray microscopy. Such very high aspect ratios would also be important for zone plates in the hard x-ray regime, where material parameters demand thicker structures for high efficiency.

[1]*Proceedings of the Seventh International Conference on X-Ray Microscopy*, edited by J. Susini, D. Joyeux, and F. Polack [J. Phys. IV **104**, (2003)].

[2]D. Attwood, *Soft X-Rays and Extreme Ultraviolet Radiation* (Cambridge University Press, Cambridge, 1999), p. 337–394.

[3]J. Kirz, J. Opt. Soc. Am. **64**, 301 (1974).

[4]E. Di Fabrizio, F. Romanato, M. Gentill, S. Cabrini, B. Kaulich, J. Susini, and R. Barret, Nature (London) **401**, 895 (1999).

[5]G. Schneider, Appl. Phys. Lett. **71**, 2242 (1997).

[6]E. H. Anderson, IEEE J. Quantum Electron. **42**, 27 (2005).

[7]D. L. Olynick, E. H. Andersson, B. Harteneck, and E. Verklerov, J. Vac. Sci. Technol. B **19**, 2896 (2001).

[8]D. Weiss, M. Peuker, and G. Schneider, Appl. Phys. Lett. **72**, 1805 (1998).

[9]W. Chao, B. D. Harteneck, J. A. Liddle, E. H. Andersson, and D. T. Attwood, Nature (London) **435**, 1210 (2005).

[10]M. Peuker, Appl. Phys. Lett. **78**, 2208 (2001).

[11]A. Holmberg, S. Rehbein, and H. M. Hertz, Microelectron. Eng. **73–74**, 639 (2004).

[12]M. Schlesinger and M. Paunovic, *Modern Electroplating*, 4th ed. (Wiley, New York, 2000), p. 13–15.

[13]L. T. Romankiw, Electrochim. Acta **42**, 2985 (1997).

[14]S. Rehbein, A. Holmberg, and H. M. Hertz, J. Vac. Sci. Technol. B **22**, 1118 (2004).

[15]M. Born and E. Wolf, *Principles of Optics*, 4th ed. (Cambridge University Press, Cambridge, 1999), p. 54–74 and p. 735–758.

[16]S. Rehbein and G. Schneider, in *Proceedings of the Eighth International Conference on X-Ray Microscopy*, Institute of Pure and Applied Physics (Japan) Conference Series 7 (2006), p. 103.